Electronic Supplementary Information

Variable coordination of tris(2-pyridyl)phosphine and its oxide toward $M(hfac)_2$: a metal-specifiable switching between the formation of mono- and bis-scorpionate complexes

Alexander V. Artem'ev,*[a] Alexey V. Kashevskii,[b] Artem S. Bogomyakov,[c] Alexander Yu. Safronov,[b] Anastasiya O. Sutyrina,[d] Anton A. Telezhkin[d] and Irina V. Sterkhova[d]

[a] *Nikolaev Institute of Inorganic Chemistry, Siberian Branch of Russian Academy of Sciences, 3, Akad. Lavrentiev Ave., Novosibirsk 630090, Russian Federation*

[b] *Irkutsk State University, Karl Marx str., 1, 664003 Irkutsk, Russian Federation*

[c] *International Tomography Center, SB RAS, Institutskaya Str. 3A, 630090 Novosibirsk, Russian Federation*

[d] *A. E. Favorsky Irkutsk Institute of Chemistry, Siberian Branch of the Russian Academy of Sciences, 1 Favorsky Str., 664033 Irkutsk, Russian Federation*

*Author for correspondence: chemisufarm@yandex.ru (Alexander V. Artem'ev)

Table S1. Data collection and refinement parameters for **3-8**

Compound	**3**	**4**	**5**	**6**	**7**	**8**
Empirical formula	$C_{25}H_{14}CuF_{12}N_3O_4P$	$C_{25}H_{14}CuF_{12}N_3O_5P$	$C_{40}H_{26}CuF_{12}N_6O_4P_2$	$C_{25}H_{16}CoF_{12}N_3O_6P$	$C_{26}H_{14}F_{12}N_3NiO_5P$	$C_{60}H_{30}F_{36}Mn_3N_6O_{12}P_2 \cdot 2C_3H_6O$
Formula mass [g/mol]	742.90	758.89	1008.16	772.27	766.08	2053.82
Space group	$P2_1/n$	$P2_1/n$	$P2_1/c$	$P2_1$	$P2_12_12_1$	P-1
a [Å]	12.5272(11)	12.515(2)	11.3926(4)	8.7336(7)	8.8330(8)	10.5909(7)
b [Å]	15.4345(14)	15.165(3)	12.4104(4)	15.7594(12)	15.6509(15)	12.6726(9)
c [Å]	14.5163(12)	14.627(3)	14.1878(5)	11.7574(9)	21.6876(17)	16.6408(11)
α [°]	90	90	90	90	90	80.785(3)
β [°]	93.306(3)	94.549(7)	95.9020(10)	111.126(3)	90	79.387(3)
γ [°]	90	90	90	90	90	65.580(3)
V [Å^3]	2802.1(4)	2767.2(9)	1995.33(12)	1509.5(2)	2998.2(5)	1990.0(2)
Z	4	4	2	2	4	1
$D_{calcd.}$ [g·cm^{-3}]	1.756	1.824	1.678	1.700	1.697	1.714
μ [mm^{-1}]	0.955	0.973	0.736	0.740	0.817	0.658
Temperature [K]	100(2)	100(2)	100(2)	296(2)	100(2)	100(2)
Reflections collected	202919	187370	67156	42752	94343	123437
Independent reflections	8228 [R_{int} = 0.0530]	8123 [R_{int} = 0.0887]	5842 [R_{int} = 0.0623]	8842 [R_{int} = 0.0987]	8828 [R_{int} = 0.0718]	11664 [R_{int} = 0.0770]
R_1, wR_2 [$I > 2\sigma(I)$]	0.0340, 0.0830	0.0544, 0.1315	0.0401, 0.0962	0.0484, 0.0820	0.0372, 0.0760	0.0433, 0.0848
R_1, wR_2 (all data)	0.0439, 0.0881	0.0718, 0.1424	0.0545, 0.1042	0.0849, 0.0910	0.0494, 0.0802	0.0738, 0.0955
Goodness of fit	1.066	1.026	1.039	1.033	1.036	1.019

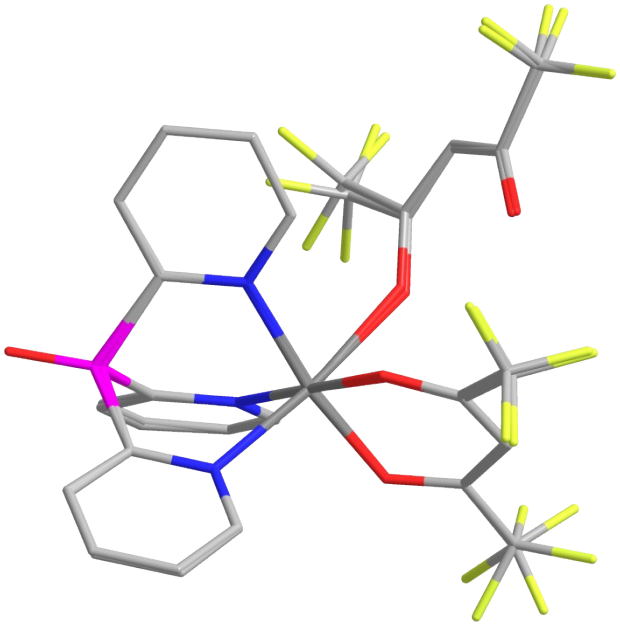

Figure S1. Overlay of the structures of [Cu(Py_3P)(*O*,*O'*-hfac)(*O*-hfac)] (**3**) and [Cu(Py_3P=O)(*O*,*O'*-hfac)(*O*-hfac)] (**4**).

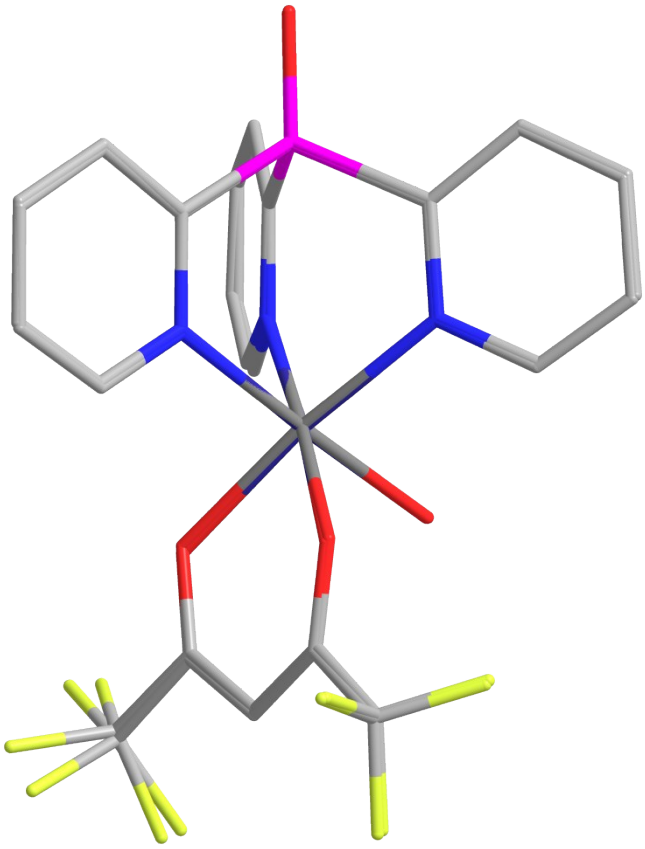

Figure S2. Overlay of the structures of [Co(Py_3P=O)(*O*,*O′*-hfac)(H_2O)](hfac) (**6**) and [Ni(Py_3P=O)(*O*,*O′*-hfac)(H_2O)](hfac) (**7**).

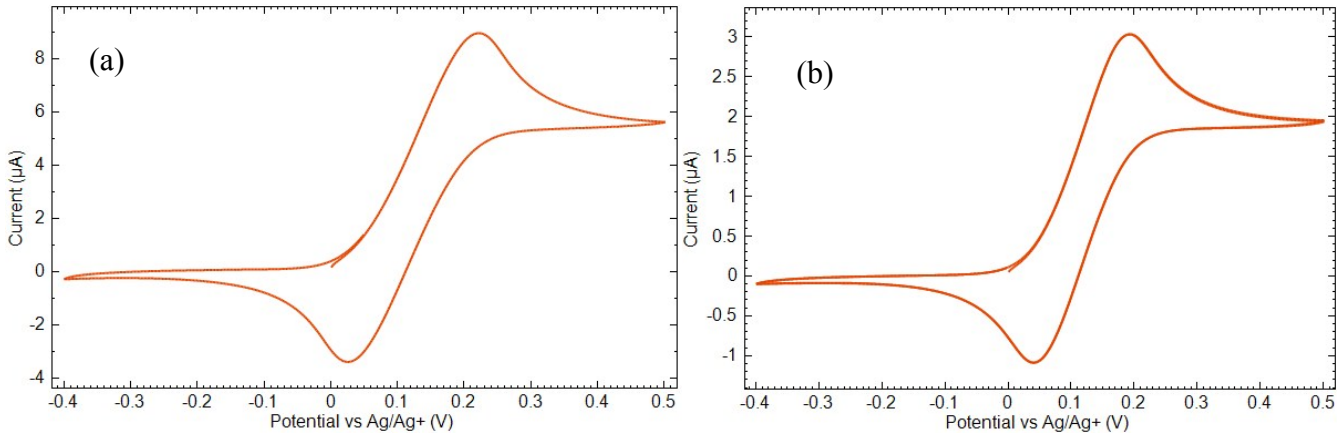

Figure S3. Cyclic voltammograms of $FeCp_2$ 10^{-3} M solution in 0.1 M TBAP in acetonitrile, measured at GC – (a) and Pt – (b) electrodes; ν = 10 mV/s.

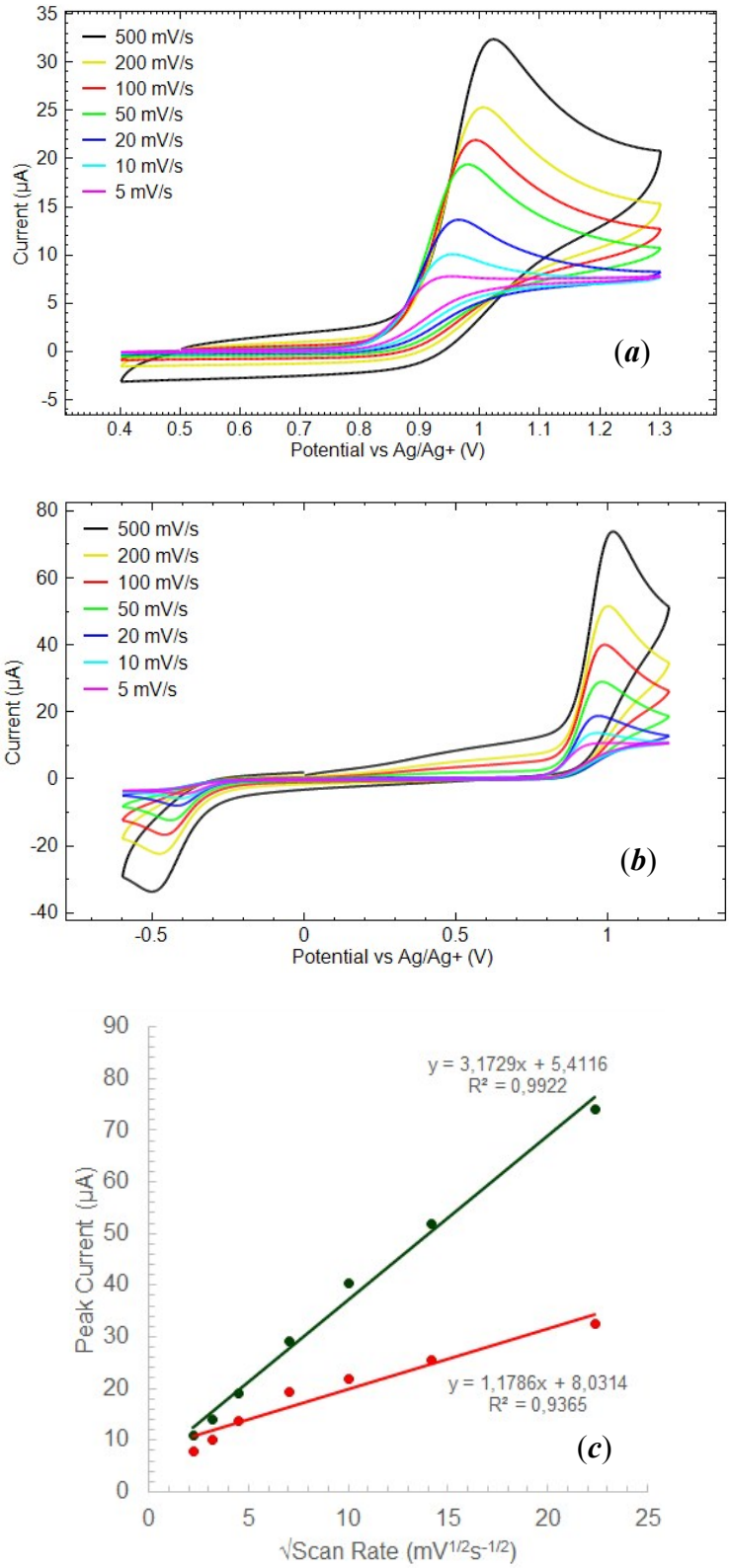

Figure S4. The influence of scan sweep rate on the cycling voltammograms of [Cu(Py_3P)(*O*,*O′*-hfac)(*O*-hfac)] (**3**) (***a***), [Cu(Py_3P)$_2$](hfac)$_2$ (**5**) (***b***), and corresponding I_{pa} *vs* $v^{0.5}$ plots (***c***).

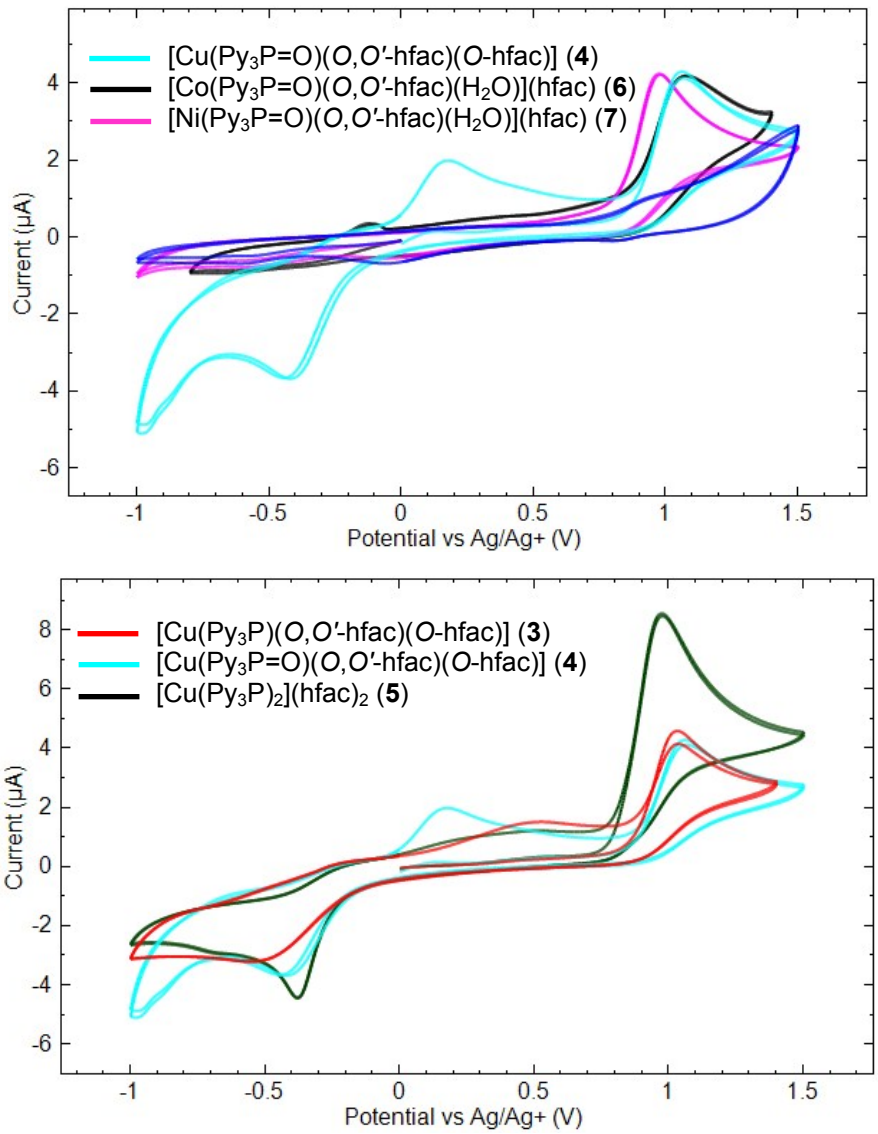

Figure S5. Cyclic voltammograms measured at Pt electrode in 0.1 M TBAP in acetonitrile solutions of 10^{-3} M complexes **4-7** (***a***) and **3-5** (***b***); (ν = 50 mV/s).

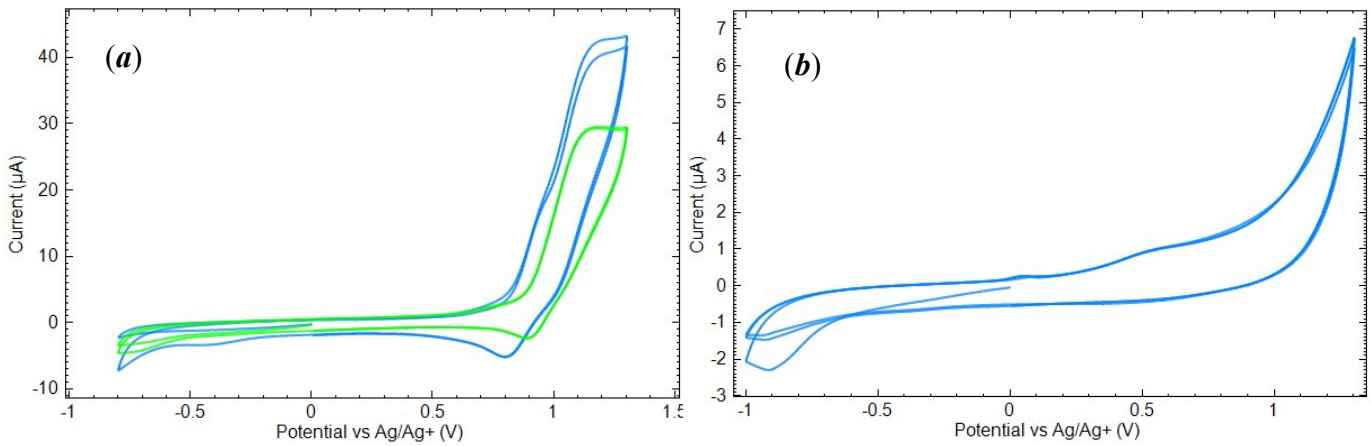

Figure S6. Cyclic voltammograms of $[Mn(Py_3P)_2][Mn(hfac)_3]_2$ (**8**) 10^{-3} M solution in 0.1 M TBAP in acetonitrile, measured at (***a***) – bare (▬) and Nafion modified (▬) GC electrode; (***b***) – Pt electrode; (ν = 50 mV/s).

Figure S7. FTIR-ATR spectrum of **[Cu(Py$_3$P)(*O*,*O'*-hfac)(*O*-hfac)]** (**3**) in range of 550-1700 cm^{-1}.

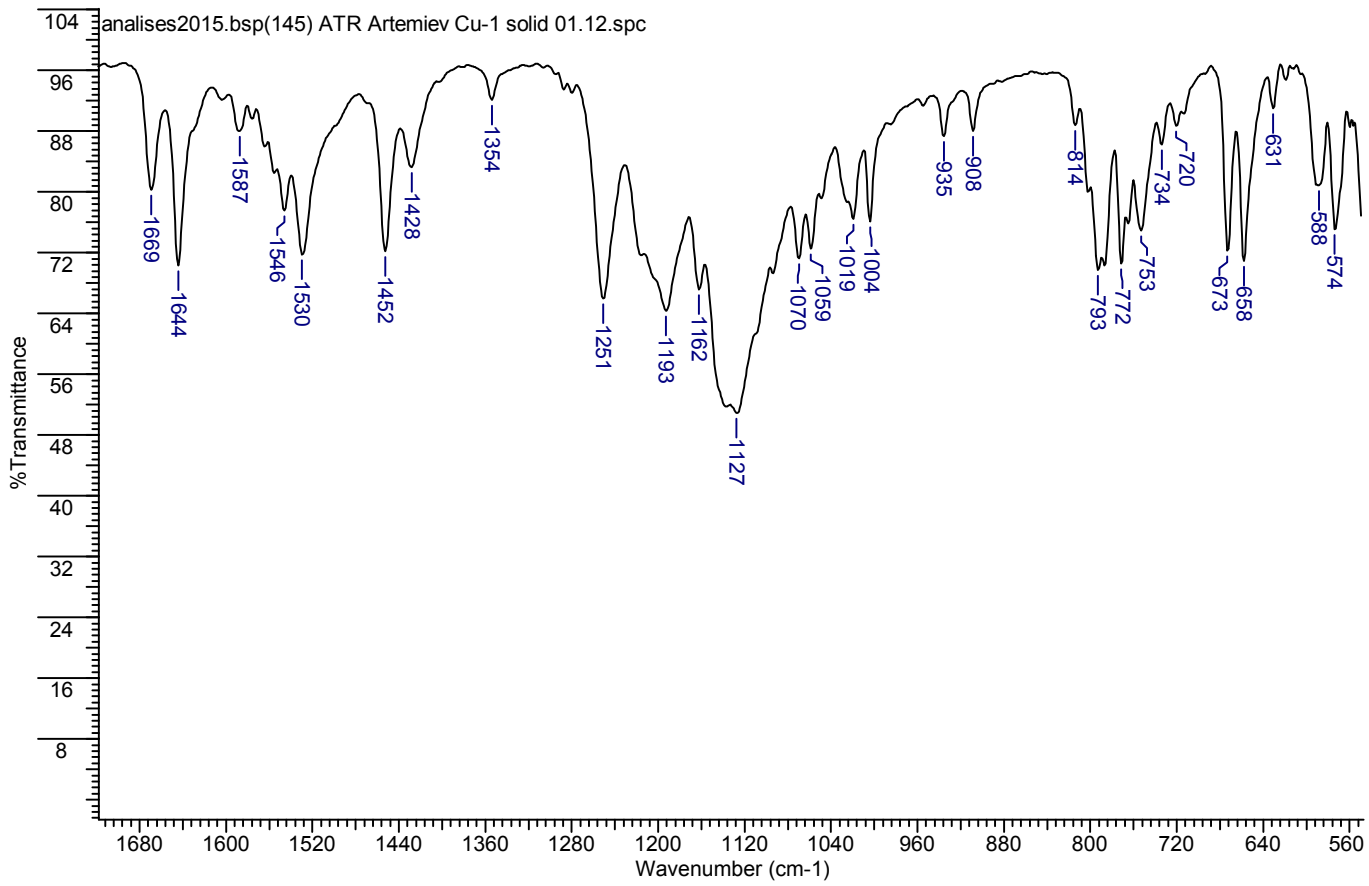

Figure S8. FTIR-ATR spectrum of **[Cu(Py$_3$P=O)(*O*,*O'*-hfac)(*O*-hfac)]** (**4**) in range of 550-1700 cm^{-1}.

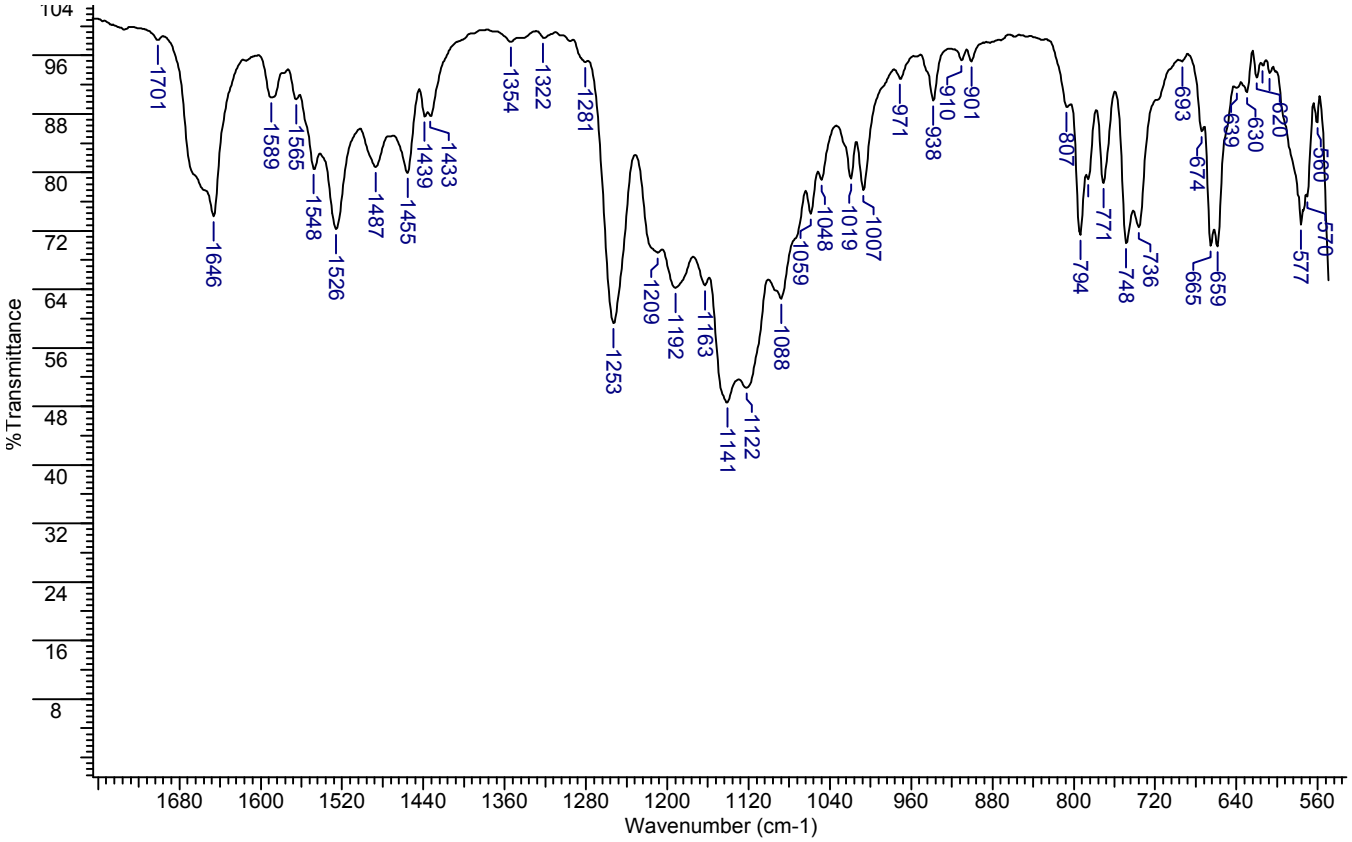

Figure S9. FTIR-ATR spectrum of **[Cu(Py$_3$P)$_2$](hfac)$_2$** (**5**) in range of 550-1750 cm^{-1}.

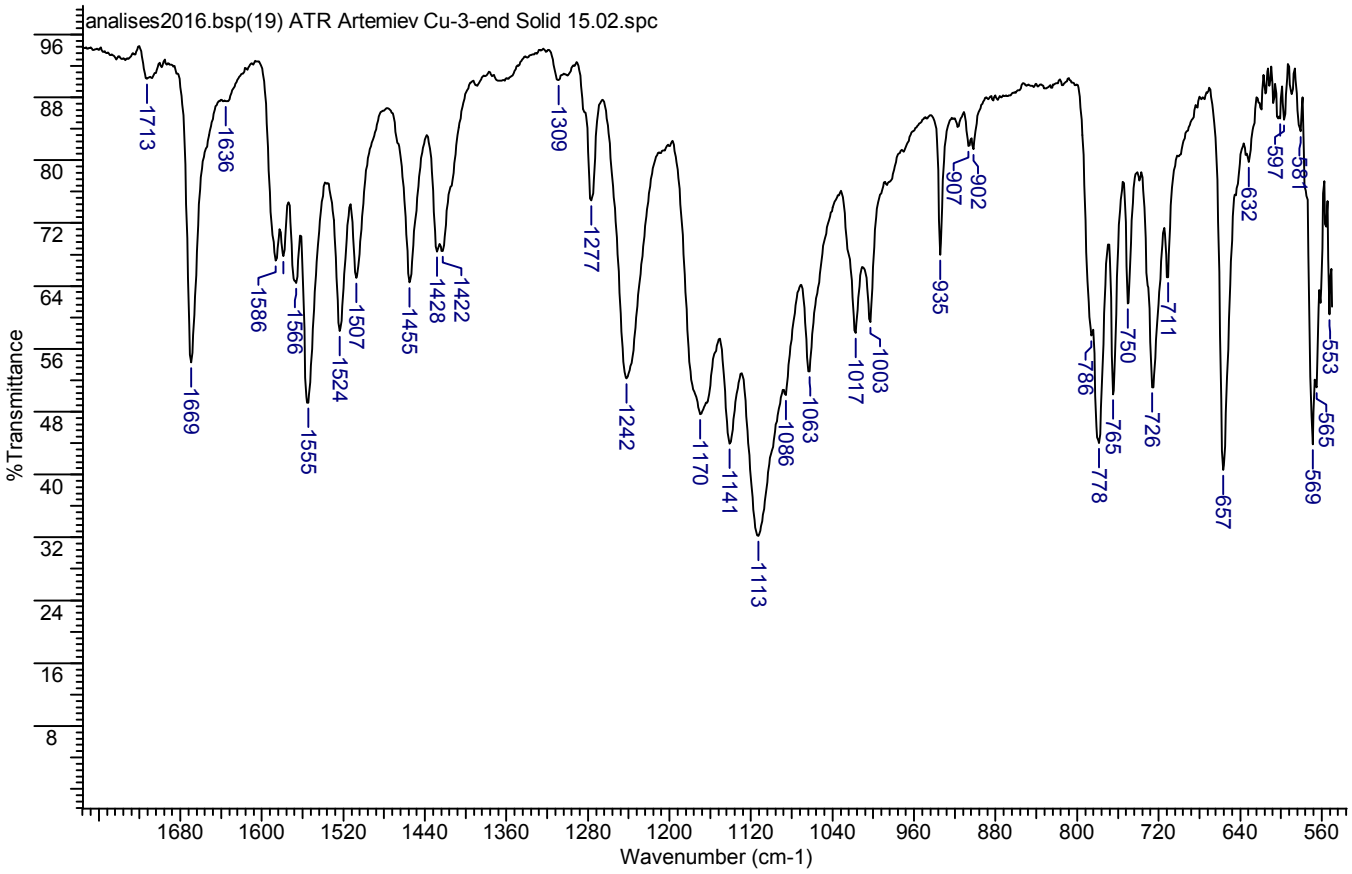

Figure S10. FTIR-ATR spectrum of **[Co(Py$_3$P=O)(*O*,*O'*-hfac)(H$_2$O)](hfac)** (**6**) in range of 500-1750 cm^{-1}.

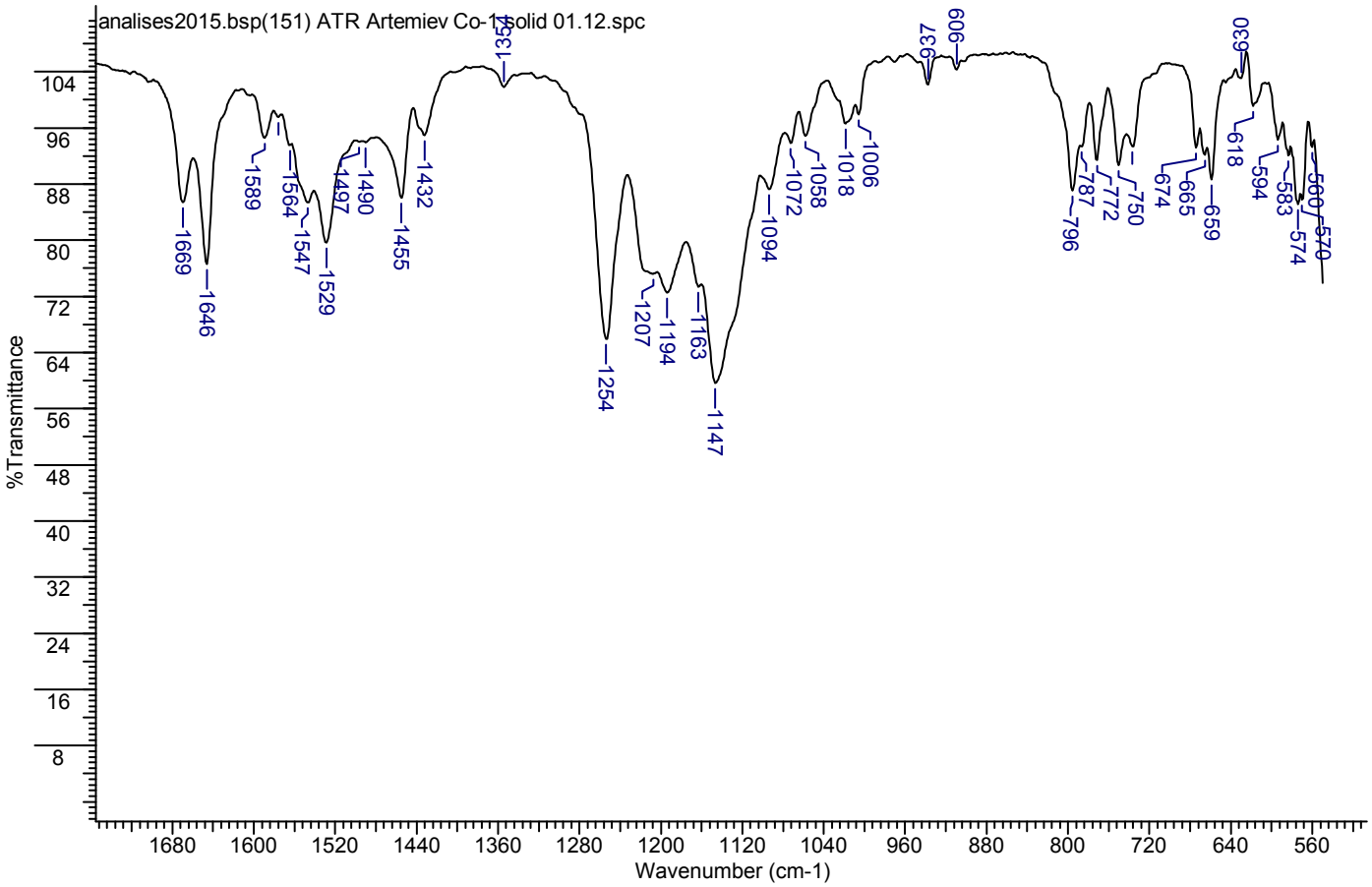

Figure S11. FTIR-ATR spectrum of **[Ni(Py$_3$P=O)(*O*,*O'*-hfac)(H$_2$O)](hfac)** (**7**) in range of 500-1750 cm^{-1}.

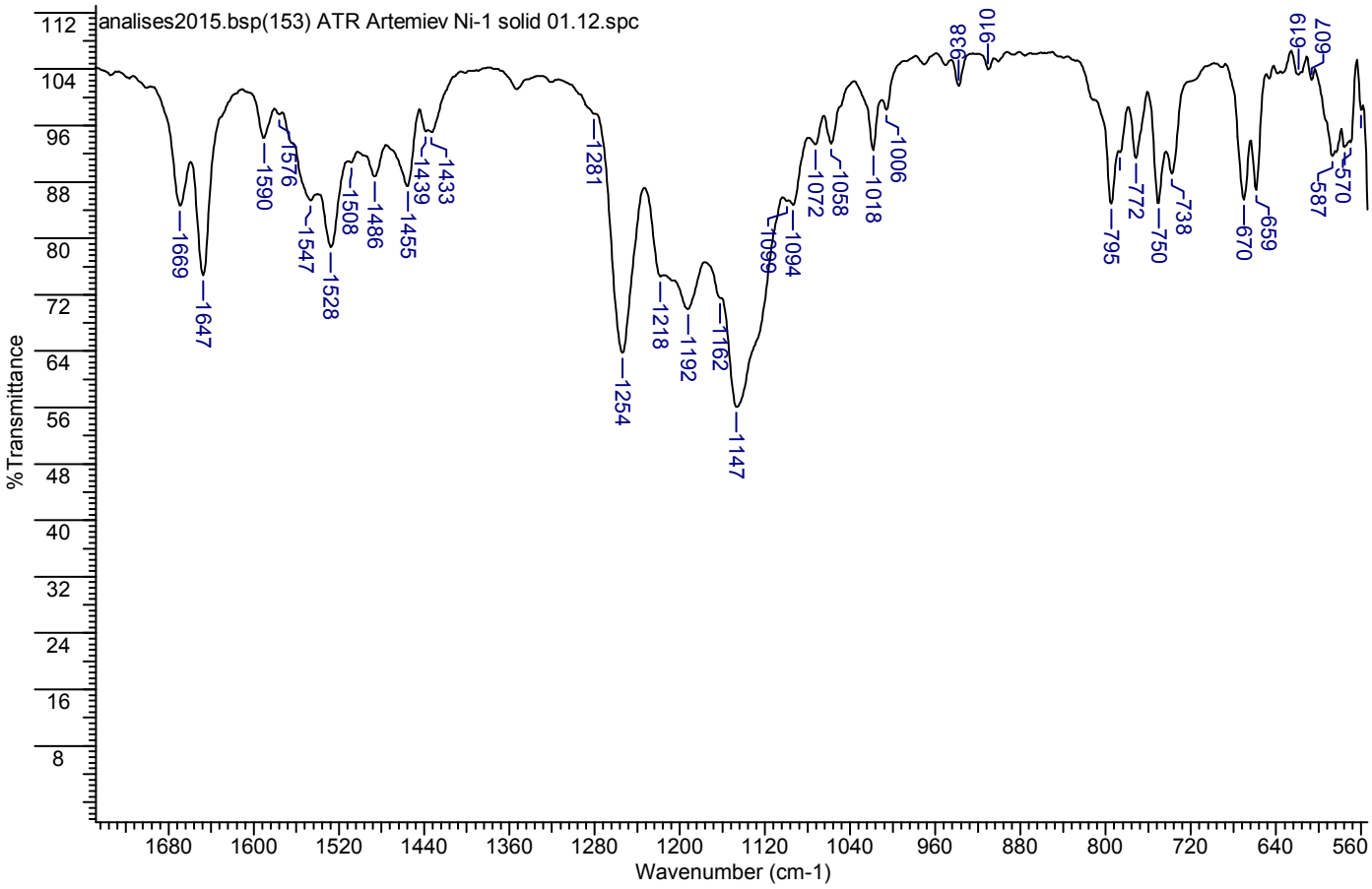

Figure S12. FTIR-ATR spectrum of [Mn(Py$_3$P)$_2$][Mn(hfac)$_3$]$_2$ (**8**) in range of 500-1750 cm^{-1}.

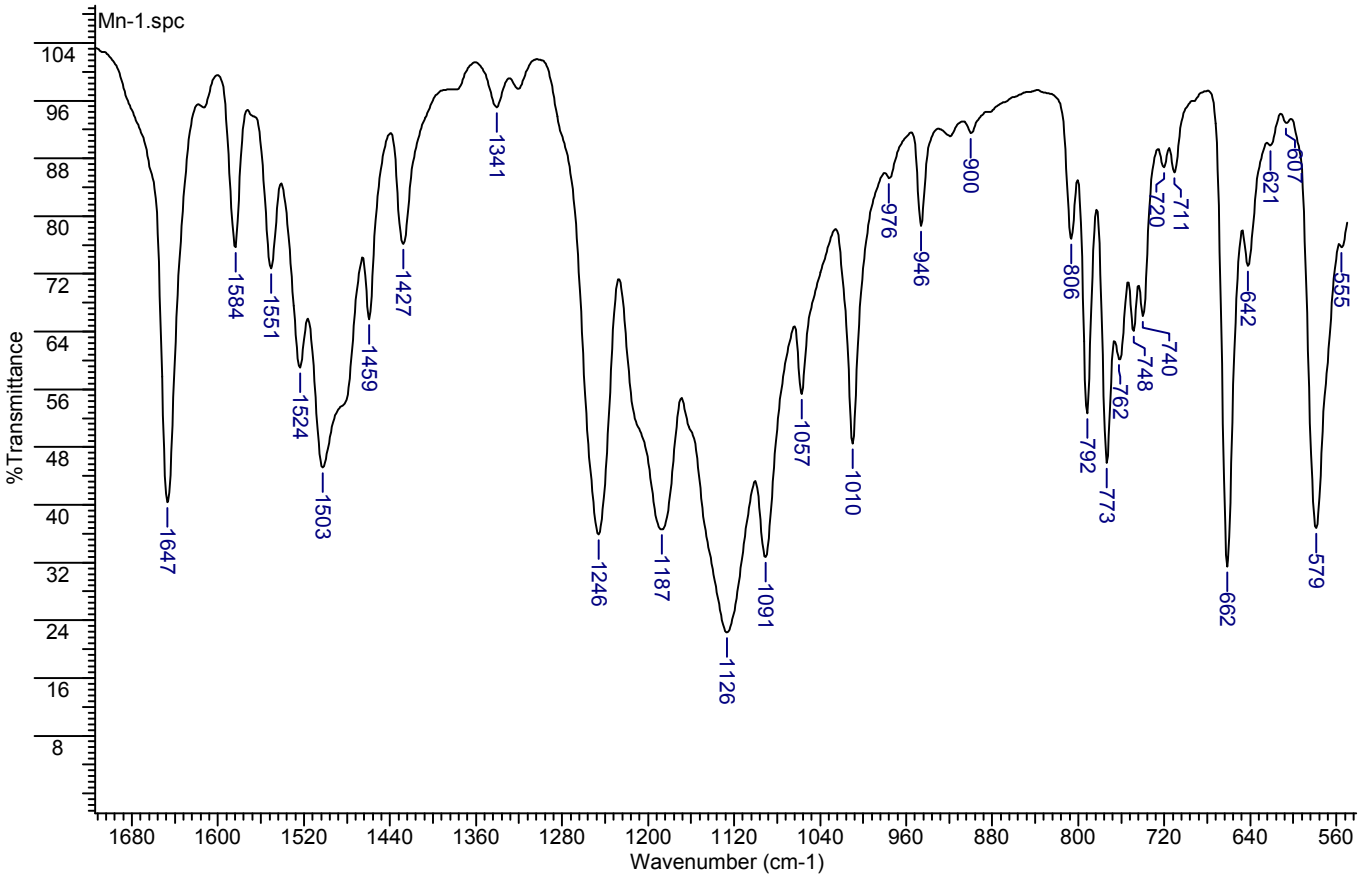

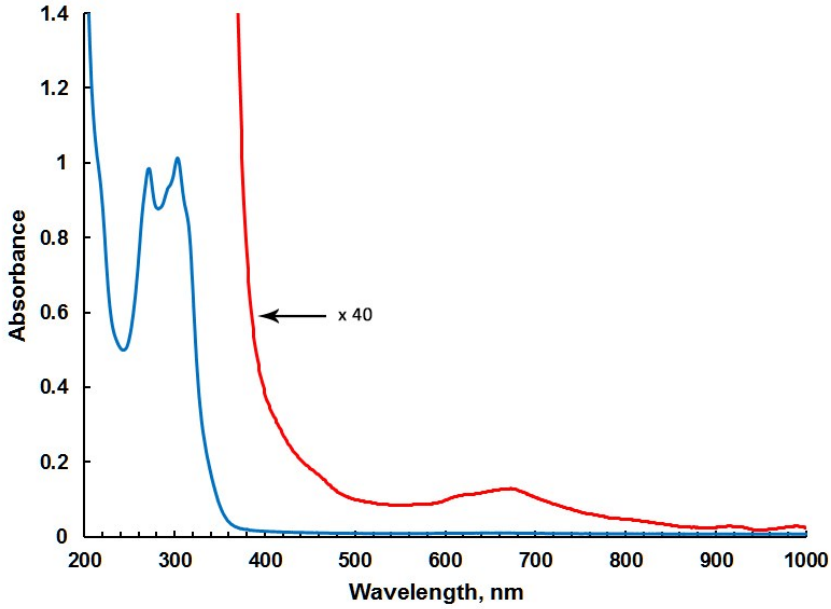

Figure S13. UV-Vis spectrum of **[Cu(Py$_3$P)(*O*,*O'*-hfac)(*O*-hfac)]** (**3**) recorded for MeCN solution.

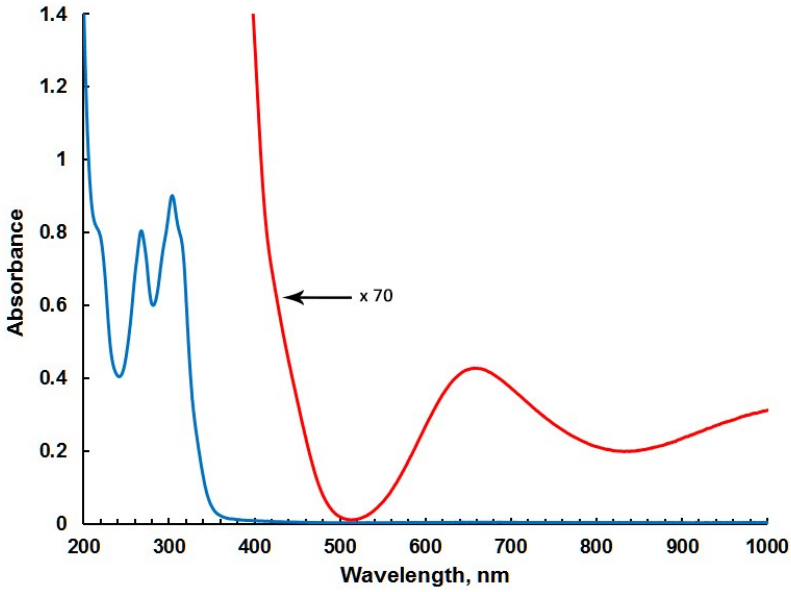

Figure S14. UV-Vis spectrum of **[Cu(Py$_3$P=O)(*O*,*O'*-hfac)(*O*-hfac)]** (**4**) recorded for MeCN solution.

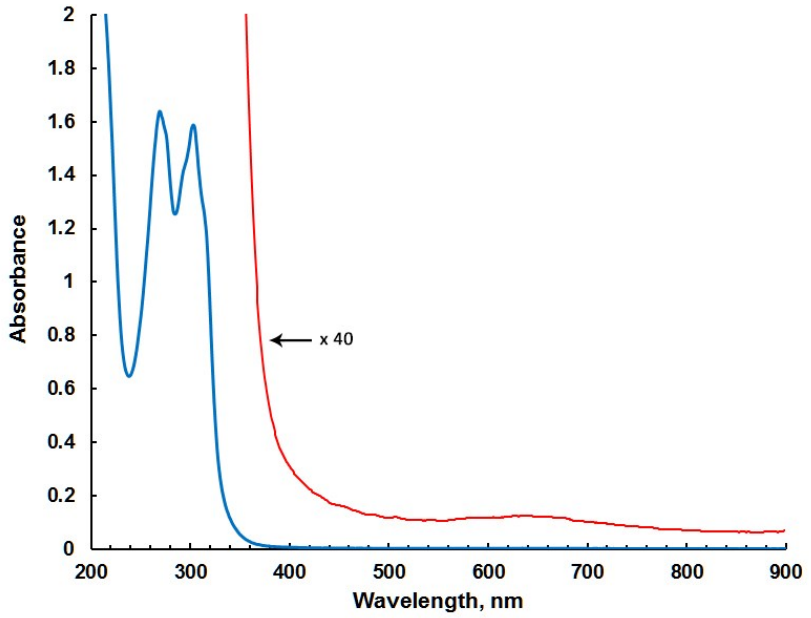

Figure S15. UV-Vis spectrum of **[Cu(Py$_3$P)$_2$](hfac)$_2$** (**5**) recorded for MeCN solution.

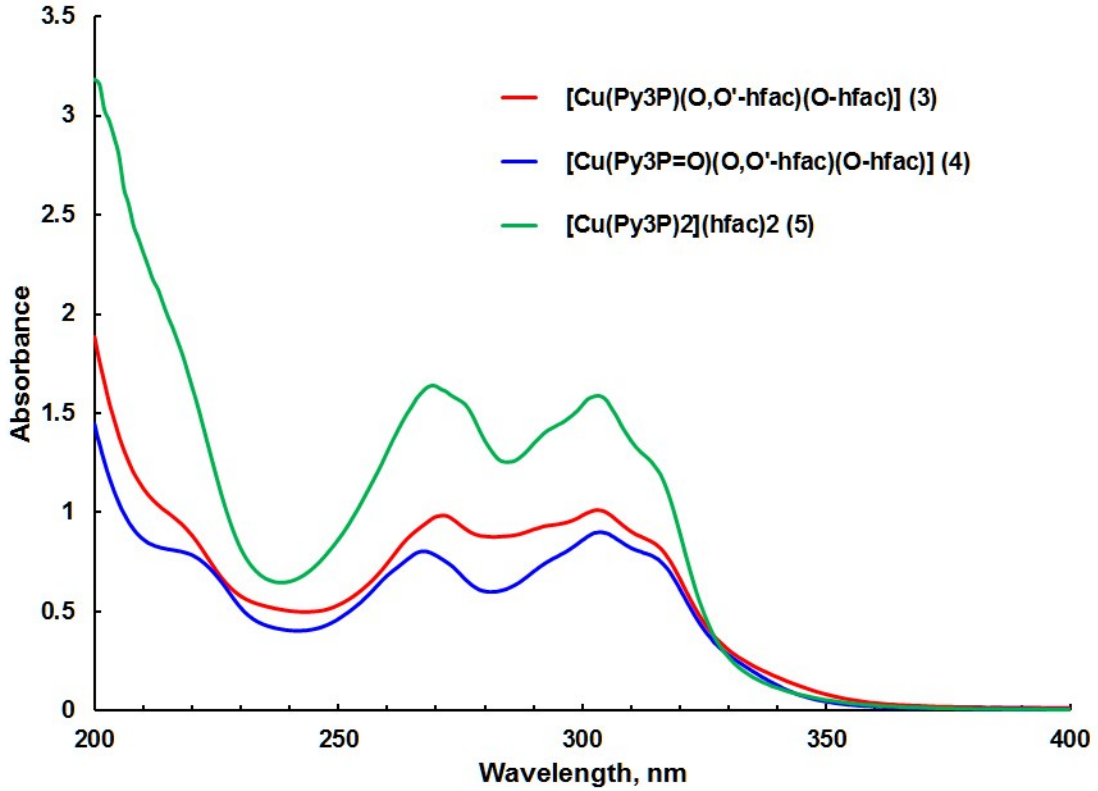

Figure S16. UV-Vis spectra of complexes **3-5** recorded for MeCN solution.

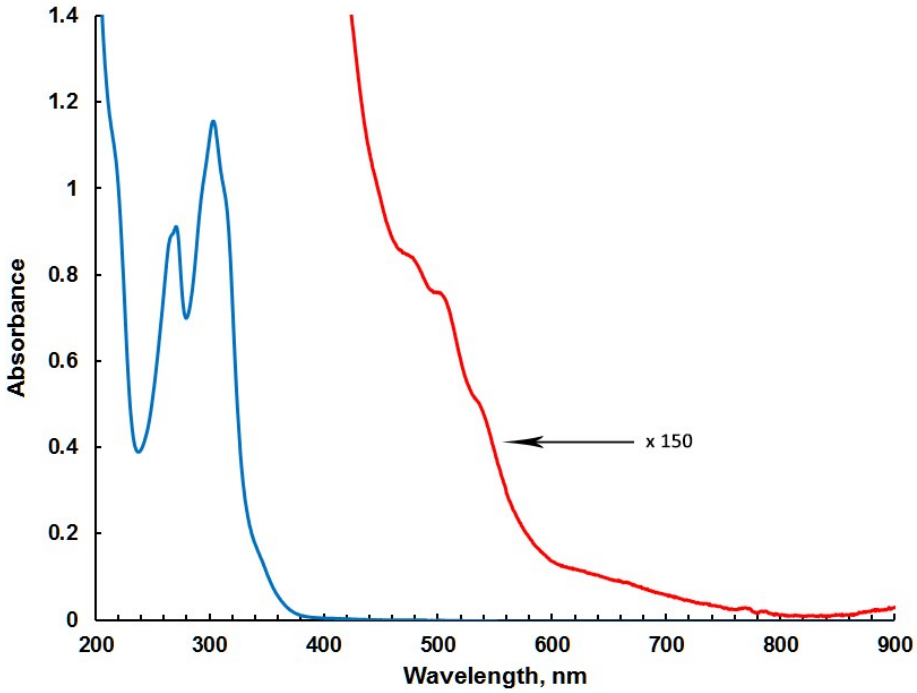

Figure S17. UV-Vis spectrum of **[Co(Py$_3$P=O)(*O*,*O'*-hfac)(H$_2$O)](hfac)** (**6**) recorded for MeCN solution.

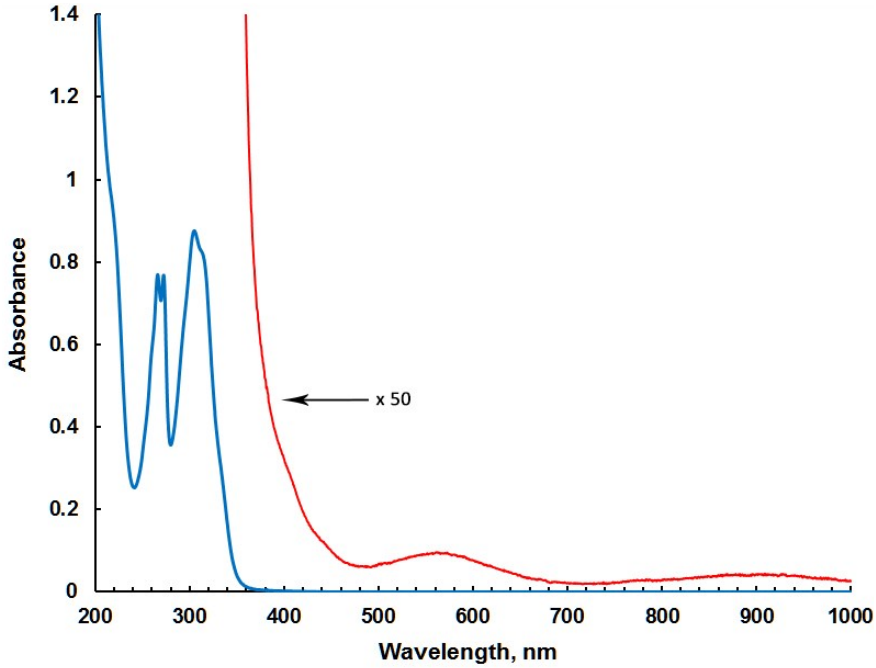

Figure S18. UV-Vis spectrum of **[Ni(Py$_3$P=O)(*O*,*O'*-hfac)(H$_2$O)](hfac)** (**7**) recorded for MeCN solution.

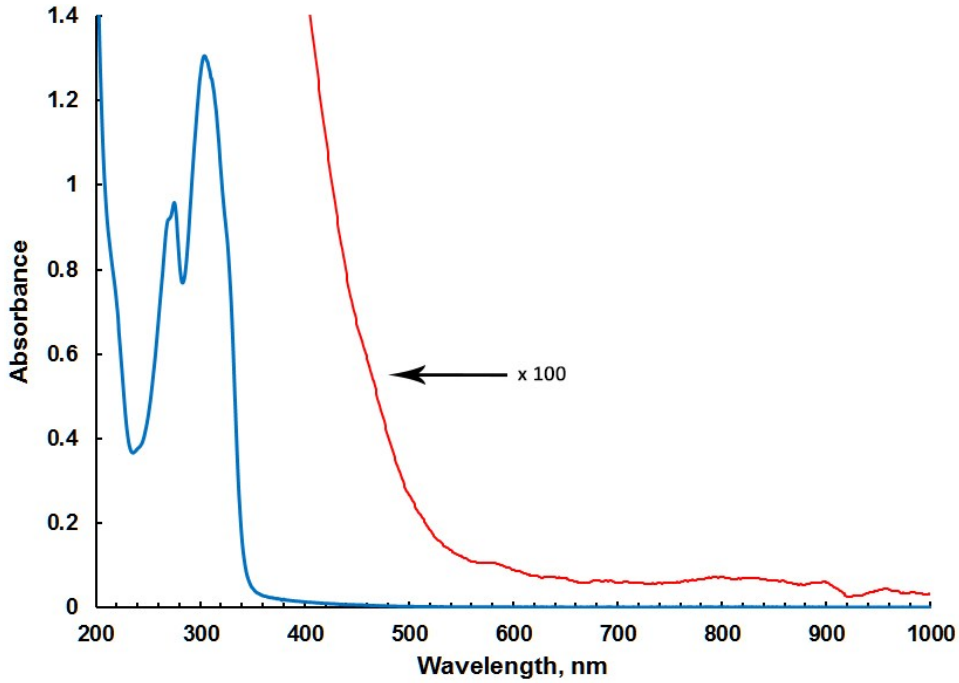

Figure S19. UV-Vis spectrum of $[Mn(Py_3P)_2][Mn(hfac)_3]_2$ (**8**) recorded for MeCN solution.

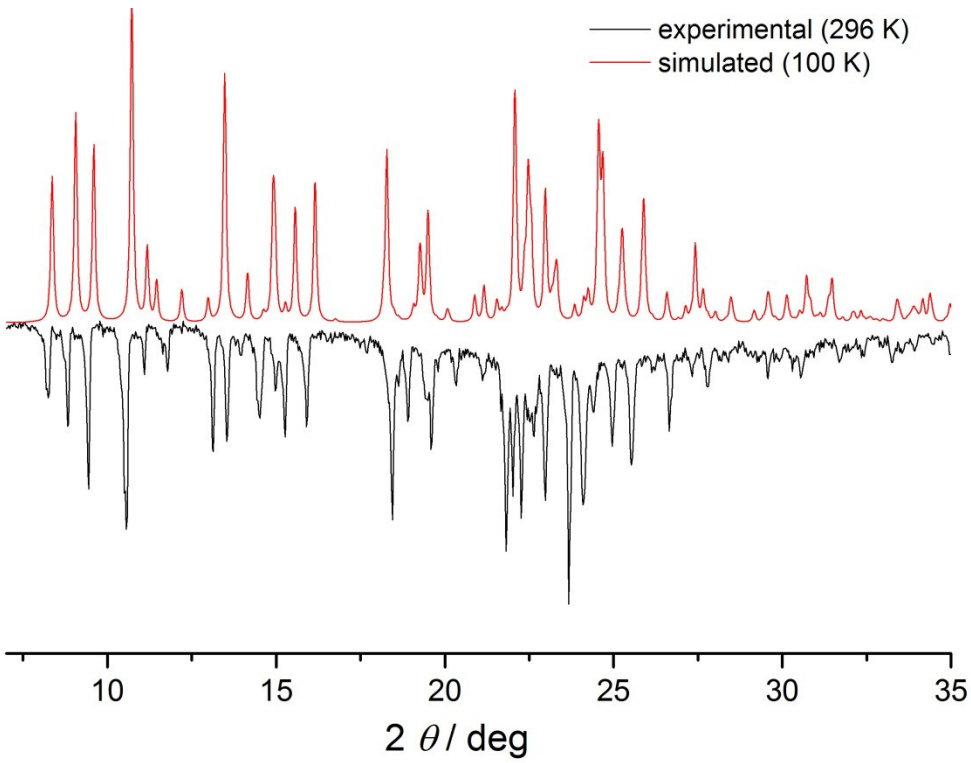

Figure S20. Experimental and simulated X-ray powder patterns for complex **3**.

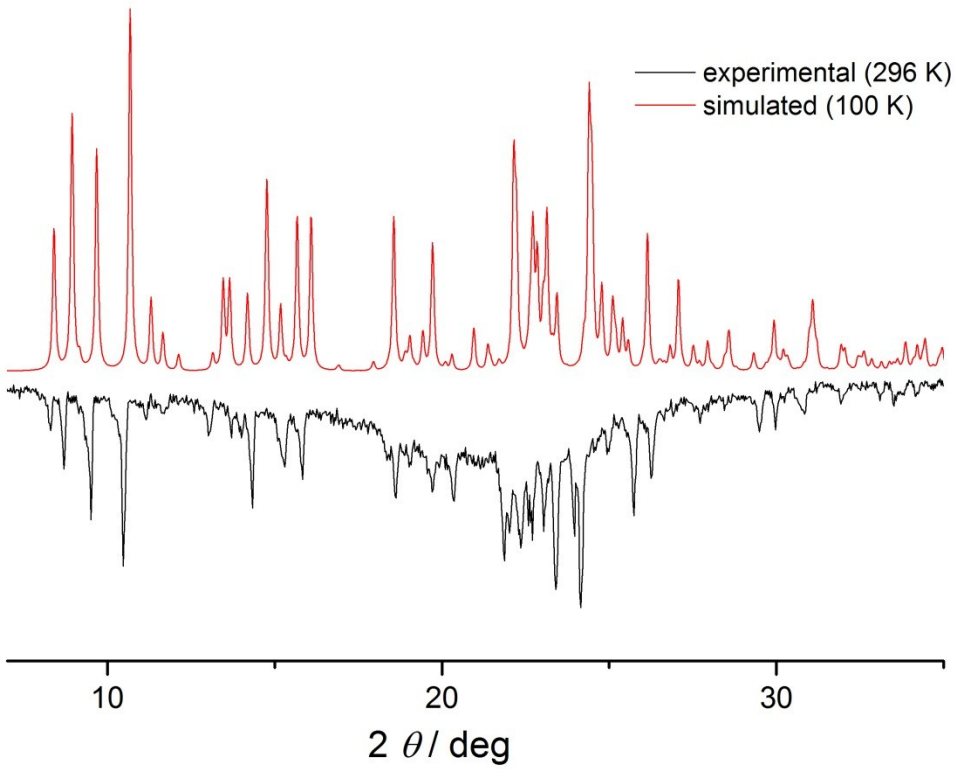

Figure S21. Experimental and simulated X-ray powder patterns for complex **4**.

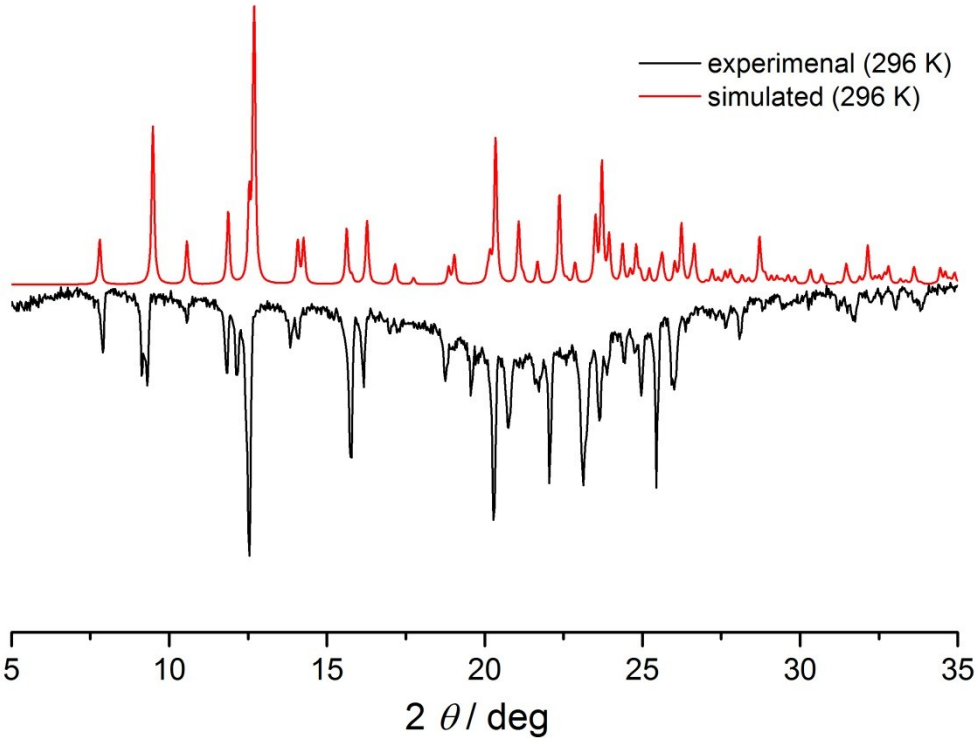

Figure S22. Experimental and simulated X-ray powder patterns for complex **5**.

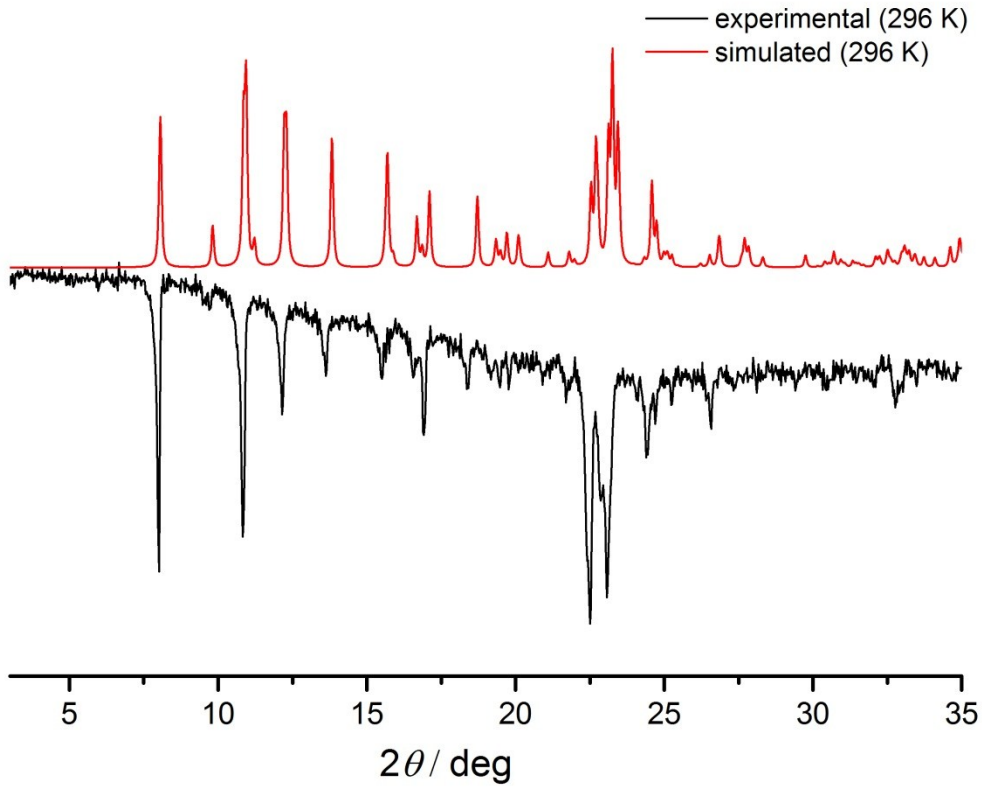

Figure S23. Experimental and simulated X-ray powder patterns for complex **6**.

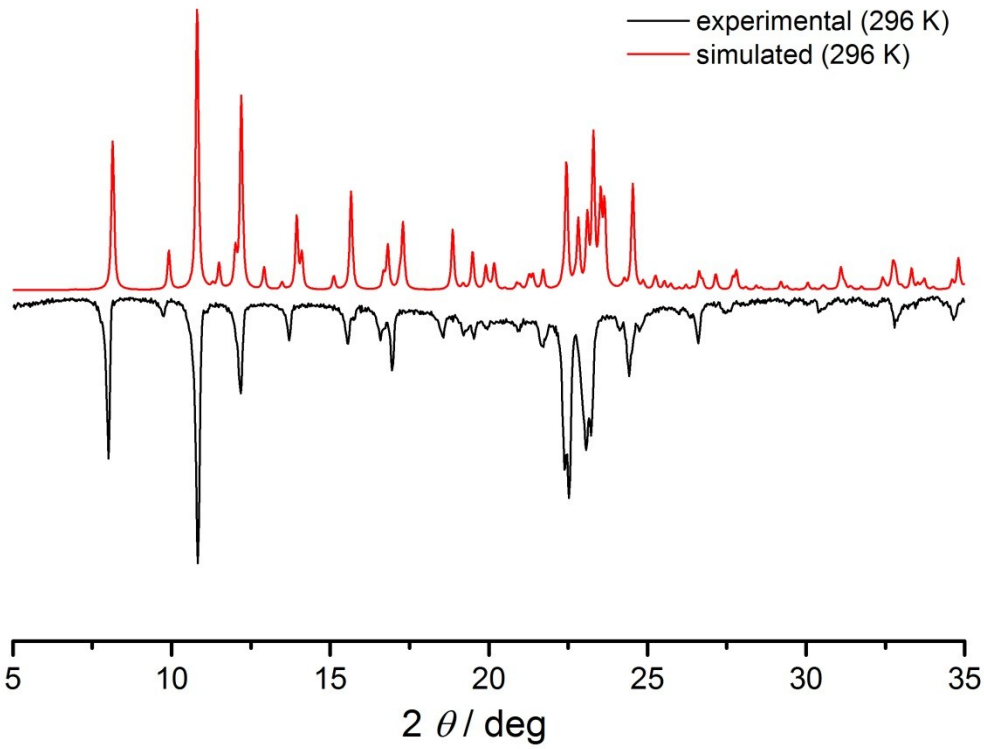

Figure S24. Experimental and simulated X-ray powder patterns for complex **7**.